Progress In Electromagnetics Research, PIER 22, 197–212, 1999

A RIGOROUS TWO-DIMENSIONAL FIELD ANALYSIS OF DFB STRUCTURES

M. Akbari, M. Shahabadi, and K. Schünemann

Arbeitsbereich Hochfrequenztechnik
Technische Universität Hamburg-Harburg
D-21071 Hamburg, Germany

1. Introduction
2. Two–Dimensional Model of Periodic Waveguides
3. Electrical Modeling of DFB Structures
4. Numerical Results and Discussions
5. Conclusions and Summary
References

1. INTRODUCTION

The wave propagation in a DFB laser (Fig. 1) primarily shows a 2-D nature. The major number of the physical characteristics of a DFB structure is directly influenced by the 2-D electromagnetic field distribution inside this structure. Consequently the common one–dimensional (1-D) models of DFB lasers based on the assumption of longitudinal wave propagation involve an inherent approximation.

The first reported analysis of a DFB laser by Kogelnik [1] is an example of a 1-D analysis utilizing coupled-wave theory. In this and also in a large variety of 1-D coupled-wave analyses, the transversal variation of the electromagnetic field is either ignored or just described approximately by a confinement factor. The evaluation of this factor and of other parameters like the coupling coefficient κ which play an important role in 1-D analyses has been studied in many different papers [2–4].

Attention has also been paid to the 2-D wave propagation in the periodic structure of a DFB laser. To our knowledge, there have been two

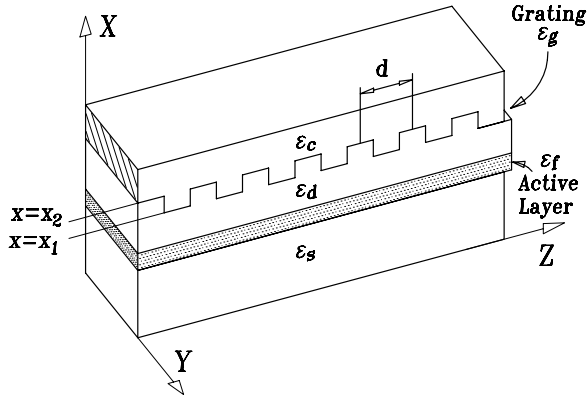

Figure 1. A typical DFB laser.

basic methods for the treatment of this problem by now, namely the modal analysis [5] and a modified 2-D coupled-wave theory [6]. In the former method, the problem of wave propagation in an infinite periodic structure is reduced to an eigenvalue problem for the modes guided by the periodic structure. The starting point of the latter method is the assumption of a set of coupled forward and backward propagating waves, so that a system of differential equations for the amplitudes of these waves describes the wave propagation.

It is the aim of this work to develop a completely different 2-D field analysis which enables us to accurately determine the field distribution in a DFB structure. For this purpose, we shall first characterize the set of waves guided by the periodic waveguide of a DFB structure. To this end we present, in accordance to our previous work [7], an electrical network the mathematical description of which coincides with the governing equations for the total field in a DFB structure. As a result, the field analysis may be reduced to a network analysis. In this case, the *natural frequencies* and their corresponding *zero-input responses* [8] of the equivalent network yield the wave numbers and the field distribution of the guided waves, respectively. This analysis can be carried out very efficiently with the help of the common methods for the analysis of electrical networks. It is worth noting that the necessary input parameters for the existing 1-D analyses, e.g., the coupling coefficient and the confinement factor, can be regarded as by-products of the method of this paper. In Section 2 we develop a basic mathematical modeling to describe the 2-D field distribution in the periodic

region of a DFB structure. With the help of this modeling, a network consisting of ideal TEM transmission lines is presented in Section 3. In the same section, we will discuss the method used to evaluate the natural frequencies and the zero-input responses of the equivalent network. Section 4 is devoted to numerical results of applying our method to some problems which have already been analyzed by other methods. Finally, we summarize the basic points of the work in Section 5.

2. TWO-DIMENSIONAL MODEL OF PERIODIC WAVEGUIDES

In this section, we will propose a method to convert Maxwell's equations inside the periodic region of a DFB structure into a system of first-order differential equations. These equations constitute the basis for a network modeling which is of primary importance in the present work.

Fig. 2 shows the periodic region of the DFB structure from Fig. 1.

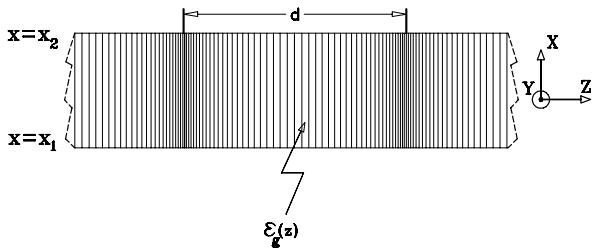

Figure 2. Geometry of a periodic layer with a period of d.

We assume no variation in y-direction $(\partial/\partial y = 0)$. Thus for TE_z-polarized waves, the y-component of the electric field E_y satisfies the wave equation

$$\frac{\partial^2 E_y(x,z)}{\partial x^2} + \frac{\partial^2 E_y(x,z)}{\partial z^2} + k_o^2 \epsilon_g(z) E_y(x,z) = 0 \tag{1}$$

where $\epsilon_g(z)$ represents the relative permittivity of the periodic region, and $k_o = 2\pi/\lambda_o$ with λ_o as free-space wavelength. The periodic variation of $\epsilon_g(z)$ can be expressed in the form of a Fourier series, i.e.,

$$\epsilon_g(z) = \sum_{m=-\infty}^{\infty} \bar{\epsilon}_m \, e^{-j2m\pi z/d} \, , \tag{2}$$

where

$$\bar{\epsilon}_m = \frac{1}{d}\int_0^d \epsilon_g(z)\, e^{+j2m\pi z/d} dz \ . \tag{3}$$

Here d means period of the variation of the dielectric constant. Regarding the periodicity of $\epsilon_g(z)$, the general solution of eq. (1) can be written as pseudo-periodic function

$$E_y(x,z) = \sum_{m=-\infty}^{\infty} \bar{E}_m(x)\, e^{-j\gamma_m z}, \ \ \gamma_m = \left(\gamma + \frac{2m\pi}{d}\right). \tag{4}$$

Solution (4) is a linear combination of terms with $\exp(-j\gamma_m z)$ called space harmonics in analogy to the common time-harmonic functions. The values of γ_m correspond to the wave numbers of these space harmonics.

The magnetic field $H_z(x,z)$ can be expressed in the same form

$$H_z(x,z) = \sum_{m=-\infty}^{\infty} \bar{H}_m(x) e^{-j\gamma_m z}. \tag{5}$$

If we define $\mathcal{E}_y(x)$ and $\mathcal{H}_z(x)$ as vectors consisting of the expansion coefficients $\bar{E}_m$ and $\bar{H}_m$ in eqs. (4) and (5), we obtain after substituting eqs. (2), (4), and (5) into Maxwell's equations

$$\frac{d}{dx}\begin{bmatrix} \mathcal{E}_y(x) \\ \mathcal{H}_z(x) \end{bmatrix} = -j\omega \begin{bmatrix} 0 & \mu_0 I \\ \epsilon_0 \mathcal{N}^2 & 0 \end{bmatrix} \begin{bmatrix} \mathcal{E}_y(x) \\ \mathcal{H}_z(x) \end{bmatrix} \tag{6}$$

with

$$\mathcal{N}^2 = \mathbf{n}^2 - \frac{1}{k_o^2}\left[\Gamma\right]^2, \tag{7}$$

where I means the identity matrix and $\mathbf{n}^2$ is defined as

$$\mathbf{n}^2 = \begin{bmatrix} \cdots & \cdots & \cdots & \cdots & \cdots & \cdots & \cdots \\ \cdots & \bar{\epsilon}_1 & \bar{\epsilon}_0 & \bar{\epsilon}_{-1} & \bar{\epsilon}_{-2} & \bar{\epsilon}_{-3} & \cdots \\ \cdots & \bar{\epsilon}_2 & \bar{\epsilon}_1 & \bar{\epsilon}_0 & \bar{\epsilon}_{-1} & \bar{\epsilon}_{-2} & \cdots \\ \cdots & \bar{\epsilon}_3 & \bar{\epsilon}_2 & \bar{\epsilon}_1 & \bar{\epsilon}_0 & \bar{\epsilon}_{-1} & \cdots \\ \cdots & \cdots & \cdots & \cdots & \cdots & \cdots & \cdots \end{bmatrix}. \tag{8}$$

$[\Gamma]$ is a diagonal matrix whose elements are the wave numbers γ_m. The system of differential equation (6) is equivalent to Maxwell's equations in the periodic region, and shows the desired form for modeling

it by an equivalent network as we will explain later. It should be noted that eq. (6) is valid in the homogeneous regions of a DFB structure as well. In those regions, where the relative permittivity is constant, the formulation can be simplified regarding the fact that all Fourier coefficients $\bar{\epsilon}_m$ in eq. (2), except for $\bar{\epsilon}_0$, are reduced to zero. In other words, the above formulation can be applied to each region of a DFB structure without any restrictions.

Solving eq. (6) for the case that the electric and magnetic fields in the plane $x = 0$ are known, we find these fields at any other plane x from

$$\begin{bmatrix} \mathcal{E}_y(x) \\ \mathcal{H}_z(x) \end{bmatrix} = [A] \begin{bmatrix} \mathcal{E}_y(0) \\ \mathcal{H}_z(0) \end{bmatrix}, \tag{9}$$

where

$$[A] = \begin{bmatrix} \cos(k_o \mathcal{N} x) & -j\eta_o \mathcal{N}^{-1} \sin(k_o \mathcal{N} x) \\ -j/\eta_0 \sin(k_o \mathcal{N} x) & \cos(k_o \mathcal{N} x) \end{bmatrix} \tag{10}$$

with $\eta_o = \sqrt{\mu_o/\epsilon_o}$. To simplify the calculation of $[A]$, one may diagonalize the matrix $\mathcal{N}$ according to

$$\mathcal{N}^2 = [P]\,[D]\,[P]^{-1}\,. \tag{11}$$

Here $[P]$ is a matrix whose columns are the eigenvectors of $\mathcal{N}^2$, whereas matrix $[D]$ is a diagonal matrix with diagonal elements λ_m^2, i.e., the eigenvalues of $\mathcal{N}^2$. Hence we introduce new vectors $\widehat{\mathcal{E}}_y(x)$ and $\widehat{\mathcal{H}}_z(x)$ according to

$$\begin{aligned} \mathcal{E}_y(x) &= [P]\,\widehat{\mathcal{E}}_y(x), \\ \mathcal{H}_z(x) &= [P]\,\widehat{\mathcal{H}}_z(x), \end{aligned} \tag{12}$$

in order to replace the vectors $\mathcal{E}_y(x)$ and $\mathcal{H}_z(x)$. After this transformation, the submatrices of $[A]$ are all diagonalized, and we arrive at

$$\begin{bmatrix} \widehat{\mathcal{E}}_y(x) \\ \widehat{\mathcal{H}}_z(x) \end{bmatrix} = \begin{bmatrix} \mathcal{A} & \mathcal{B} \\ \mathcal{C} & \mathcal{D} \end{bmatrix} \begin{bmatrix} \widehat{\mathcal{E}}_y(0) \\ \widehat{\mathcal{H}}_z(0) \end{bmatrix} \tag{13}$$

with

$$\begin{aligned} \mathcal{A} = \mathcal{D} &= [\cos(k_o \lambda_m x)] \\ \mathcal{B} &= -\left[j \frac{\eta_o}{\lambda_m} \sin(k_o \lambda_m x) \right] \\ \mathcal{C} &= -\left[j \frac{\lambda_m}{\eta_o} \sin(k_o \lambda_m x) \right]\,. \end{aligned}$$

Equation (13) is equivalent to a chain matrix representation for an infinite set of *uncoupled* transmission lines. According to eq. (13), at each point x the voltage and current of the i-th transmission line correspond to the i-th element of the vectors $\widehat{\mathcal{E}}_y(x)$ and $\widehat{\mathcal{H}}_z(x)$, respectively. The propagation constant of the i-th transmission line is given by λ_i, while its characteristic impedance reads $\eta_o/\sqrt{\lambda_i}$. We will utilize these results in the next section to develop an electrical model for a given DFB structure.

3. ELECTRICAL MODELING OF DFB STRUCTURES

Applying the mathematical modeling introduced in the previous section to a DFB structure, we will now introduce an electrical model which can be used to determine the 2-D field distribution in such a structure.

A 2-D drawing of the DFB structure of Fig. 1 is illustrated in Fig. 3(a), where a rectangular groove shape has been assumed for the periodic region or grating. Note that other groove shapes may be analyzed by subdividing the grating into a finite number of layers and approximating each of these layers by using a grating with rectangular profile.

Fig. 3(b) depicts the equivalent network of the shown structure. It consists of a set of cascaded transmission lines which are connected to multiport networks $\mathbf{T}_1$ and $\mathbf{T}_2$. The transmission lines in the periodic region $x_1 < x < x_2$ model the wave propagation in accordance with eq. (13). With regard to this equation, the characteristic admittance of the m-th transmission line is given by

$$Y_m = \sqrt{\lambda_m}/\eta_o. \tag{14}$$

In a homogeneous region, this admittance can be calculated from

$$Y_m = \sqrt{k_o^2\varepsilon_n - \gamma_m^2}/\eta_o k_o, \tag{15}$$

where ε_n $(n = s, f, d, c)$ represents the relative permittivity of the corresponding homogeneous region. In the last relation, we have taken into account that the m-th space harmonic $\exp(-j\gamma_m z)$ propagates in a region with constant relative permittivity ε_n.

The multiport networks $\mathbf{T}_1$ and $\mathbf{T}_2$ are included in the equivalent network of Fig. 3(b) in order to model the transformations at the

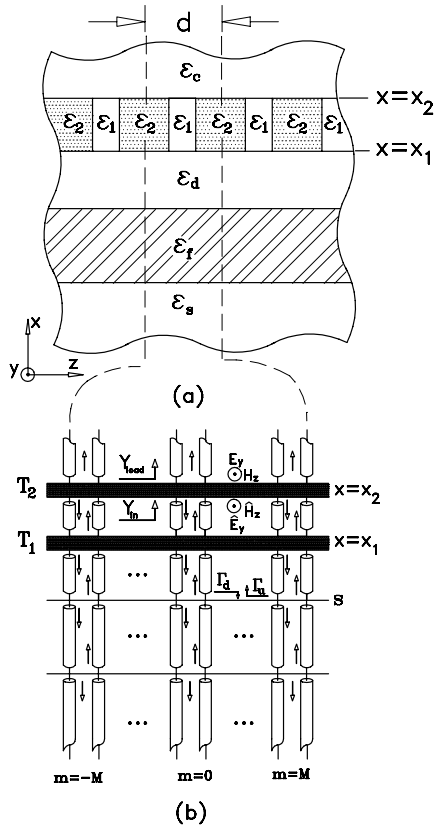

Figure 3. (a) Geometry of a general DFB structure with rectangular grating, (b) network model for one period.

interfaces of the periodic region given by eq. (12). For instance, at $x = x_2$ the network $\mathbf{T}_2$ performs the transformations $\mathcal{E}_y(x = x_2^+) = [P]\,\widehat{\mathcal{E}}_y(x = x_2^-)$ and $\mathcal{H}_z(x = x_2^+) = [P]\,\widehat{\mathcal{H}}_z(x = x_2^-)$.

The relation between $\mathcal{E}_y(x = x_2^+)$ and $\mathcal{H}_z(x = x_2^+)$ can be established by determining the admittances at $x = x_2$ when looking into positive x-direction (see Fig. 3(b)). This leads to

$$\mathcal{H}_z(x = x_2^+) = [Y_{\text{load}}]\,\mathcal{E}_y(x = x_2^+) \tag{16}$$

with an admittance matrix $[Y_{\text{load}}]$. The vector transformation carried out by $\mathbf{T}_2$ maps this admittance matrix into the matrix

$$[Y_{\text{in}}] = [P]^{-1}\,[Y_{\text{load}}]\,[P]\ , \tag{17}$$

which is comparable to the function of a transformer. Matrix $[Y_{\text{in}}]$ relates the voltages and currents in the periodic region according to

$$\widehat{\mathcal{H}}_z(x = x_2^-) = [Y_{\text{in}}]\, \widehat{\mathcal{E}}_y(x = x_2^-)\,. \tag{18}$$

Equations (14) to (18) constitute a complete characterization of the network model in Fig. 3(b). Using these relations, we will now analyze the equivalent network in order to determine the set of guided modes and their corresponding propagation constants.

Since the natural frequencies of this network correspond to the propagation constants of the DFB structure, we should determine the zero-input response of the network. To this end, the network is divided into two parts, e.g., at plane S in Fig. 3(b). The upward and downward propagating waves are terminated at this plane with reflection matrices $[\Gamma_u]$ and $[\Gamma_d]$, respectively. Thus the continuity of voltages and currents at plane S requires

$$\det([\Gamma_d]\,[\Gamma_u] - I) = 0, \tag{19}$$

what constitutes a dispersion relation for the waves guided by the DFB structure. The values of γ (see eq. (4)) which satisfy eq. (19) form the set of possible propagation constants.

On the other hand, any eigenvector of the product $[\Gamma_d]\,[\Gamma_u]$ with corresponding eigenvalue of unity can be thought to represent the zero-input response of the equivalent network. These eigenvectors determine the incident waves of the transmission lines at that plane at which the above product is defined. Starting with these incident waves, one is able to evaluate the voltages and currents of the equivalent network at any x which determine the expansion coefficients $\bar{E}_m(x)$ and $\bar{H}_m(x)$ in eqs. (4) and (5), respectively. Substitution of the obtained expansion coefficients in eqs. (4) and (5) leads to the required 2-D field distributions $E_y(x, z)$ and $H_z(x, z)$ of each mode guided by the DFB structure.

4. NUMBERICAL RESULTS AND DISCUSSIONS

In the following, the developed network modeling is applied to the analysis of some practical DFB structures.

As first example, we examine the propagation characteristics of the thin-film structure shown in the insert of Fig. 4. This structure has

been analyzed in [5, 9] by a modal analysis which is based on a Hill differential equation studied in [10]. Fig. 4 shows the results obtained by our method in comparison with those computed by a perturbational method and by the method of [9]. Note the excellent agreement of the numerical results of this work with those reported in [9].

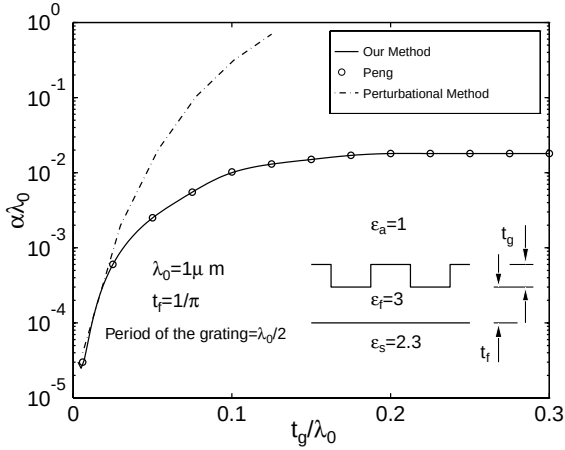

Figure 4. Variation of the attenuation factor α versus grating thickness t_g. d is the period of the grating.

The diagram of Fig. 4 shows the imaginary part of the propagation constant γ for the lowest propagating mode as function of grating thickness t_g. We have assumed $\gamma = \beta - j\alpha$ so that α represents an attenuation constant in the direction of propagation. Damping can be caused either by radiation or by the Bragg effect in the vicinity of the stop band. In the particular example of Fig. 4, radiation has caused the shown attenuation since the working frequency is far from the stop band (i.e., $\Lambda \neq m\lambda_g/2$, where m is an integer number, characterizing the order of the grating, Λ and λ_g are the period of the grating and the wavelength of the guided wave, respectively).

The expansions (4) and (5) have been truncated in the numerical analysis. By retaining only coefficients with $m = -M$ up to $m = M$, we have realized that even a value of $M = 7$ leads to fast relative convergence.

Periodic structures have found a broad spectrum of applications in the field of integrated optics, e.g., in filter structures. The filtering property of periodic structures is basically a result of the presence

of stop-bands where the longitudinal wave number becomes complex. In this case, the incident wave decays exponentially and is reflected backward. To show this property, we consider the structure illustrated in Fig. 5.

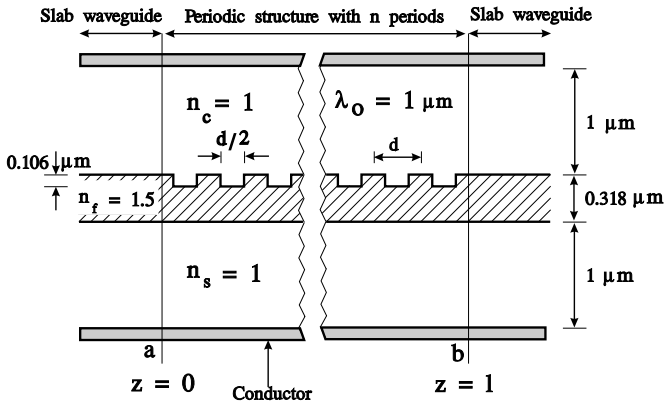

Figure 5. A typical filter used in integrated optics. The periodic structure is terminated by two dielectric slab waveguides.

In this filter, the periodic waveguide fills the region $0 < z < l$ which is terminated by two dielectric slab waveguides extending in regions $z \leq 0$ and $z \geq l$. To determine the transmission characteristic of this filter, we expand the total field inside the periodic waveguide in terms of the set of all waves guided by the structure. This expansion is matched in planes a and b of Fig. 5 to a similar expansion for the slab waveguides. In the course of that matching, we pay attention to the transversal components of both electric and magnetic fields.

Since the filter of Fig. 5 has a shielded construction, the spectrum of the guided waves is discrete. In the following computations, we have considered 10 modes of this spectrum for both the slab waveguides and the DFB structure. In Fig. 6, the computed transmission and reflection characteristics of this filter are shown as a function of the grating period for a free-space wavelength of $\lambda_o = 1\mu$m. The number of periods in the DFB structure is assumed to be 20.

As can be seen, this passive DFB structure has a characteristic like that of a band-stop filter for frequencies at which the Bragg condition is fulfilled. The 2-D electric field distribution is visualized in Fig. 7 for the case that the grating period amounts to $d = 0.41\mu$m and that

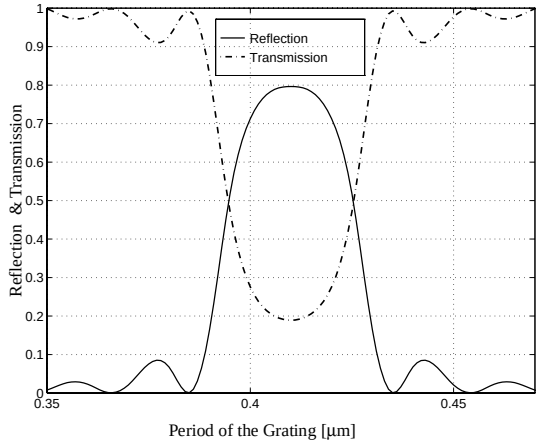

Figure 6. Reflection and transmission characteristics of the filter illustrated in Fig. 5 versus the grating period for 20 periods.

the DFB structure contains 10 periods. As can be seen in Fig. 7, the electric field decays exponentially while propagating in z-direction. Note also that the standing wave on the left hand side is caused by the reflected wave. Moreover, the distributed nature of the reflected wave can be recognized in Fig. 7 clearly.

Fig. 8 shows a structure to be considered next. It is an example of an active structure used in a DFB laser. In this laser, the active layer is characterized by its relative permittivity ε_f and its gain g_o per unit length. The effective gain parameter computed by our method is seen in Fig. 8 in comparison with the computed values using the method proposed by Wang [11, 12].

His results which are based on a truncated Floquet representation of the total field considerably deviate from those given by the 2-D method of this work because the model of [11] does not take into account the mode conversion at the junction of two succeeding steps of the grating thus leading to an inaccuracy in the final results.

As final example, we examine a Multi-Quantum-Well (MQW)-DFB laser. There is an increasing interest in the applications of MQW-DFB lasers, which is partly owing to the fact that MQW laser diodes show the desirable characteristics of a low threshold current and a tunable lasing wavelength by modifying the structure of the quantum well layers [13]. The selected MQW-DFB laser has 10 active quantum well layers each of which is buried between two barrier layers (passive

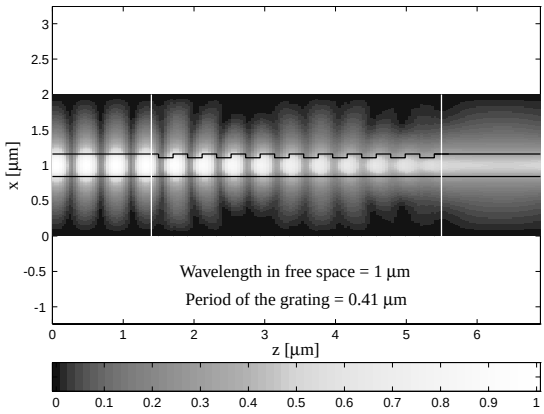

Figure 7. The two-dimensional field distribution of the structure illustrated in Fig. 5 for 10 periods.

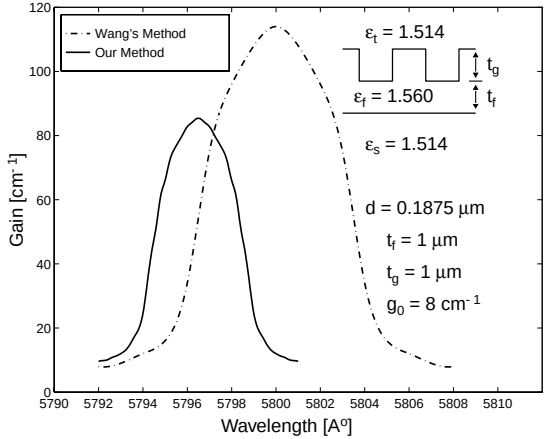

Figure 8. Gain (imaginary part of the propagation constant) for the structure shown in the insert calculated by our method (solid line) and by Wang's model (dashed line). d and g_o are period of the grating and the gain of the active layer ($\epsilon_f = 1.560$), respectively.

quantum well layers). Its lasing wavelength amounts to $\lambda_o = 1532nm$. The grating has a period of 235 nm and a duty cycle of 35%. Table 1 summarizes other parameters of this structure.

Firstly, we have calculated the attenuation of the structure in the Bragg region for the first and second order of the grating. The results

Layer	Thickness [nm]	Refracting Index
1	1000	3.162
2	40	3.381
$3, 5, 7, \ldots 23$	4.8	3.381
$4, 6, 8, \ldots 22$	7.8	3.595
24	57	3.381
25	45	3.165
26	28	3.256
27	1000	3.156

Table 1. Parameters of the simulated MQW–DFB structure.

of this simulation can be seen in Fig. 9.

The attenuation is maximum at the Bragg-wavelength. The maximum of this attenuation which is related to the coupling coefficient κ and to the bandwidth of the Bragg region, decreases for the second order of the grating to about 43% of its value for the first order. Fig. 10 shows the normalized distribution of the transversal electric field. The refractive indices of different regions of the quantum well layers (active and passive) as well as that of the grating layer are also depicted.

As can be seen, the electric field is maximum in the quantum well layers and decays exponentially towards the substrate and top layers. For this structure, the computed effective index of refraction, i.e., $n_{eff} = \lambda_o/\lambda_g$ where λ_g represents the guide wavelength, amounts to 3.256 . Figs. 11 and 12 are visualizations of the 2-D electric field distribution inside the structure of Fig. 10. From the total 2-D distribution of the electric field, we can calculate the confinement factor. This factor, which represents the fraction of the total intensity in the active region of the laser, is defined according to

$$\Gamma = \frac{\int_{actice} E_y^2(x)dx}{\int_{-\infty}^{\infty} E_y^2(x)dx}. \tag{20}$$

The simulated confinement factor for the shown structure is about $\Gamma = 0.15$.

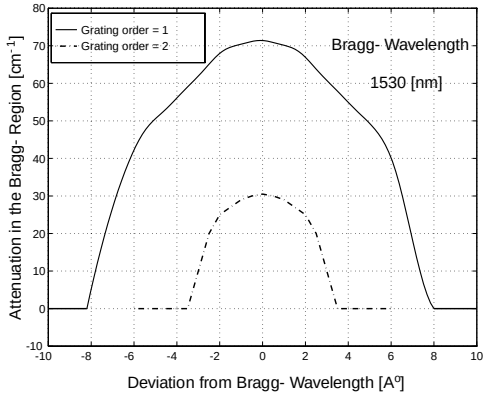

Figure 9. Computed attenuation of the MQW structure of Table 1 in the Bragg region.

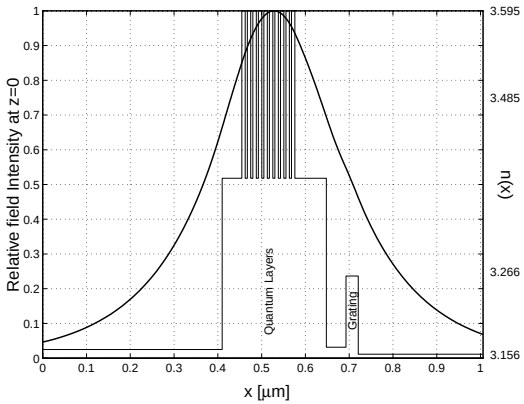

Figure 10. Transversal electric field distribution for the first order of the grating of the MQW structure characterized in Table 1.

5. CONCLUSIONS AND SUMMARY

In this work, we have developed a network of ideal transmission lines, the voltages and currents of which satisfy a system of differential equations analog to 2-D Maxwell's equations governing the electromagnetic field in a DFB structure. The parameters of this network can directly be determined from the physical parameters of the DFB structure to be investigated.

To determine the propagation constants of the set of waves guided by the DFB structure, we analyze the equivalent network for zero-input

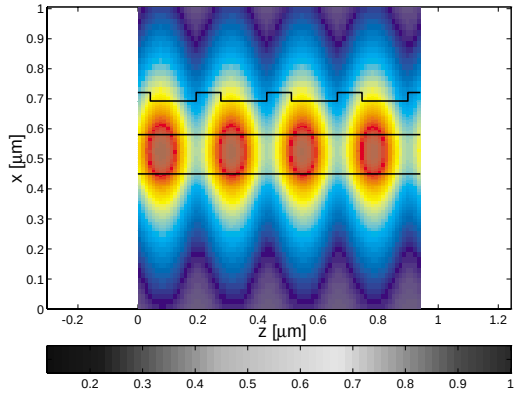

Figure 11. 2-D electric field distribution inside the investigated MQW structure for first order of the grating.

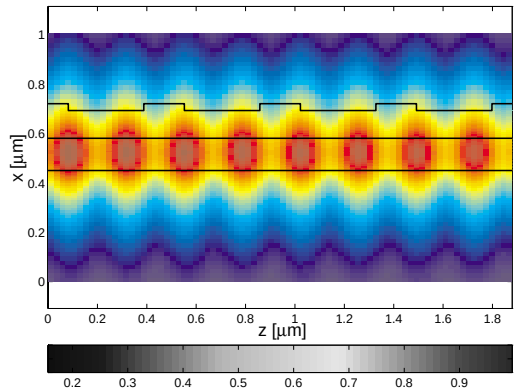

Figure 12. 2-D electric field distribution inside the investigated MQW structure for second order of the grating.

response which leads to a dispersion relation for the guided waves. The steps of this analysis can be carried out very efficiently. Moreover, the equivalent network may be applied to any arbitrary DFB structure without any restriction on its physical parameters.

We have shown that the application of this 2-D method leads to results with higher accuracy in comparison with those obtained by the common 1-D analyses of DFB structures. The reason for that is the possibility of a precise modeling of all scattering phenomena contributing to the wave propagation in a DFB structure.

ACKNOWLEDGMENT

The authors gratefully acknowledge Dr. H. Burkhard from Deutsche Telekom AG, Technologiezentrum Darmstadt, for fruitful discussions.

REFERENCES

1. Kogelnik, H. and C. V. Shank, "Coupled-wave theory of distributed feedback lasers," *J. Appl. Phys.,* Vol. 43, 2325–2335, 1972.
2. Streifer, W., R. D. Burnham, and D. R. Scifres, "Coupling coefficients and propagation constants in guided wave distributed feedback lasers," *J. Appl. Phys.,* Vol. 46, 946–948, 1975.
3. Streifer, W., D. R. Scifres, and R. D. Burnham, "Coupling coefficients for distributed feedback and single- and double-heterostructure diode lasers," *IEEE J. Quantum Electron.,* Vol. QE-11, 867–873, 1975.
4. Yariv, A., "Coupled-mode theory for guided-wave optics," *IEEE, J. Quantum Electron.,* Vol. QE-9, 919–933, 1973.
5. Peng, S. T., H. L. Bertoni, and T. Tamir, "Analysis of periodic thin-film structures with rectangular profiles," *Optics Comm.,* Vol. 10, 91–94, 1974.
6. Sato, H. and Y. Hori, "Two-dimensional theory of distributed feedback semiconducture lasers," *IEEE, J. Quantum Electron.,* Vol. QE-26, 467–472, 1990.
7. Shahabadi, M. and K. Schünemann, "Millimeter-wave holographic power splitting/combining," *IEEE, Trans. Microwave Theory Tech.,* Vol. MTT-45, 2316–2323, 1997.
8. Desoer, C. A. and E. S. Kuh, *Basic Circuit Theory,* Ch. 14, McGraw-Hill, 1969.
9. Handa, K., S. T. Peng, and T. Tamir, "Improved perturbation analysis of dielectric gratings," *Appl. Phys. Lett.,* Vol. 5, 325–328, 1975.
10. Lewis, L. R. and H. Hessel, "Propagation characteristics of periodic arrays of dielectric slabs," *IEEE, Trans. Microwave Theory Tech.,* Vol. MTT-19, 276–286, 1971.
11. Wang, S., "Proposal of periodic layered waveguide structures for distributed lasers," *J. Appl. Phys.,* Vol. 44, 767–780, 1973.
12. Wang, S., "Principles of distributed feedback and distributed Bragg reflector lasers," *IEEE, J. Quantum Electron.,* Vol. QE-10, 413–424, 1974.
13. Zory, P. S., "Quantum well lasers," *Academic Press Inc.,* 1993.